Kinematic Analysis and Optimum Design of a Novel 2PUR-2RPU Parallel Robot

Yaojun Wang[a,b], Bruno Belzile[c], Jorge Angeles[c], Qinchuan Li[a,*]

[a] *Faculty of Mechanical Engineering and Automation, Zhejiang Sci-Tech University, Hangzhou 310018, Zhejiang Province, China*
[b] *Department of Electrical and Electronic Engineering, Zhejiang Institute of Mechanical and Electrical Engineering, Hangzhou 310053, Zhejiang Province, China*
[c] *Department of Mechanical Engineering and Centre for Intelligent Machines, McGill University, Montreal, QC H3A 0C3, Canada*

Abstract

A three-dof 2PUR-2RPU redundantly-actuated parallel-kinematics machine, designed for the machining of complex curved surfaces that require high-speed and high-precision, is the object of study in this paper. The lower-mobility PKM, consisting of two pairs of symmetric, limited-dof limbs, has the advantages of high stiffness, simple kinematic chain, and reduced singularities. The mobility of the robot is investigated via Lie-groups, instead of the well-known Chebyshev-Grübler-Kutzbach formulas, which are not applicable to our case. Then, the inverse-displacement, direct-displacement and corresponding velocity relations are analyzed in detail. Next, by investigating the rank-deficiency of the corresponding Jacobian, three types of singularities, those associated with direct-kinematics, inverse-kinematics and combinations thereof, are analyzed in depth, while constraint singularities are investigated by resorting to constraint wrenches. Moreover, the workspace of both the reference point P and the tool head, when a tool is added to the moving platform, are derived. It is noteworthy that the local and global dexterity indices are evaluated by resorting to the characteristic length to homogenize the dimensionally inhomogeneous Jacobian matrix at hand, then the condition number is minimized over the independent posture parameters and the characteristic length via the first-order normality conditions.

Keywords: Parallel-kinematics machine, actuation redundancy, kinematics, Lie-groups, workspace, dexterity

*Corresponding author
Email addresses: bluepi@126.com (Yaojun Wang), bruno@cim.mcgill.ca (Bruno Belzile), angeles@cim.mcgill.ca (Jorge Angeles), lqchuan@zstu.edu.cn (Qinchuan Li)

1. Introduction

It is known that parallel-kinematics machines (PKMs), comprised of one or multiple kinematic chains, are attracting more and more attention in both academia and industry [1]. A comprehensive enumeration of parallel-kinematics machines and their applications, up to 2006, was provided by Merlet [2]. A more recent account is available in Chapter 18 of th Springer Handbook of Robotics [3]. However, the disadvantages of smaller workspace, limited dexterity and singularity issues are obstacles in the application of PKMs, although they are slowly finding their way into various application environments [3].

In the machining of workpieces with complex curved surfaces, lower-mobility 2R1T[1] PKMs, integrated either with a two-to-three degree-of-freedom (dof) tool head or a two-dof gantry to form five-to-six dof hybrid kinematic machines, have been considerably researched and subsequently applied. The Tricept [4], Z3 head [5], Exechon [6, 7], and A3 head [8] are typical examples of successful applications in the machining industry, which requires high speed and precision. Other applications include medical, such as minimally invasive surgery [9] and lower-limb rehabilitation [10], which have the exact desired motion pattern, namely, roll, pitch, and heave, as the PKM under study.

In response to the applications, many type-synthesis methods of 2R1T PKMs were introduced, such as screw theory [11, 12], Lie-groups [13, 14], and conformal geometric algebra [15]. With the methods at hand, a variety of mechanisms were designed and investigated, such as 3-PRS [16], 3-CUP [17], 3-CRS/PU [18], 3-PUU [19], Tex3 [20], 2PRU-UPR [21], and 3-CRC [22], where P, R, S, C, U stand for prismatic, revolute, spherical, cylindrical, and universal joint, respectively.

Compared with the aforementioned 2R1T PKMs without actuation redundancy, their redundantly actuated counterparts offer several advantages [23]. Indeed, actuation redundancy of overconstrained PKMs can further improve rigidity and precision, while eliminating certain types of singularities. Based on the effect of the redundant active joints on the mobility of a mechanism, PKM redundancy can be basically classified into two types. When the active joints introduce a mobility higher than what is required, the mechanism is said to be kinematically redundant; otherwise, the robot is redundantly actuated [24, 25]. Many a study, however, focuses on actuation redundancy, with an ever increased interest on stiffness and on an improved quality of manipulator workspace [25, 26, 27, 28, 29].

It should be noted that the design of a redundantly actuated lower-mobility PKM with limbs of limited dof[2] is a challenging task [30]. Although adding a six-dof limb to a PKM without changing the mobility of the PKM is an easy task, it is difficult to maintain the original mobility after adding a limited-mobility limb. To the best of our knowledge, the types of redundantly actuated reduced-mobility PKMs with limited-dof limbs are currently rare. A brief list

[1] R: rotation; T: translation

[2] A limb is said to be of limited dof if it is supplied with less than six dof as an open chain.

was provided by Xu et al. [30]. To fill the gap, a redundantly actuated 2PUR-2RPU 2R1T PKM is proposed here, where actuated joints appear underlined. When this PKM is used as a machine tool targeting complex curved surfaces, it offers several advantages over their counterparts. First, two of its actuators driving the prismatic joints are mounted on the base, which reduces the movable mass, thereby improving the dynamic response of the mechanical system. Moreover, its architecture is symmetric, with two pairs of identical PUR and RPU limbs, the former being composed of two cross links with the benefit of eliminating Type-II singularities. Additionally, the chain has a simple kinematic model and a higher stiffness. Last, but not least, the same PKM offers an improved workspace. Despite all the said benefits, redundantly actuated PKMs are subjected to several challenges. The first is the generation of internal forces introduced by redundant actuation, which leads to control requirements that cannot be satisfied with ordinary position-control schemes [31]. Moreover, motion control and mechanism calibration, among other challenges, should be taken into consideration when designing and applying redundantly actuated PKMs [32].

Performance evaluation is a key issue in the optimum design of PKMs. Most performance indices, such as manipulability and condition number, tell algebraic characteristics of the Jacobian matrix of a PKM, i.e., the dexterity of the robot [33, 34]. However, when computing the Jacobian condition number, required to assess the robot dexterity, the disparate units of the matrix in question prevent the computation of its norm. To cope with this problem, a *characteristic length* [33] is introduced.

The paper is organized as follows: We describe first the 2PUR-2RPU PKM and analyze its mobility using Lie algebra in Section 2, followed by the inverse-displacement and direct-displacement analyses in Sections 3. After the velocity analysis in Section 4, four singularity types, namely, direct-kinematics, inverse-kinematics, combined singularity, and constraint singularities, are analyzed in detail in Section 5. Considering the physical constraints imposed by the joints, the reachable workspace is analyzed in Section 6. By resorting to the characteristic length to render the Jacobian dimensionally homogeneous, performance evaluation and dexterity analysis of the robot of interest are discussed at length in Section 7. Finally, some remarks are given, together with the conclusions, in Section 8.

2. Description, Notation, and Mobility Analysis

2.1. Description and Notation

As shown in Figs. 1–3, the 2PUR-2RPU PKM is composed of a base platform (BP), two identical PUR and two identical RPU limbs, both pairs actuated at the corresponding P joint, and a moving platform (MP). The ith limb for $i = 1, 2, 3, 4$, is $A_iB_iC_i$.

As shown in Fig. 1, a Cartesian coordinate frame, $\mathcal{B}(X, Y, Z)$, is attached to the fixed base at the intersection O of the lines B_1B_2 and C_3C_4. A moving

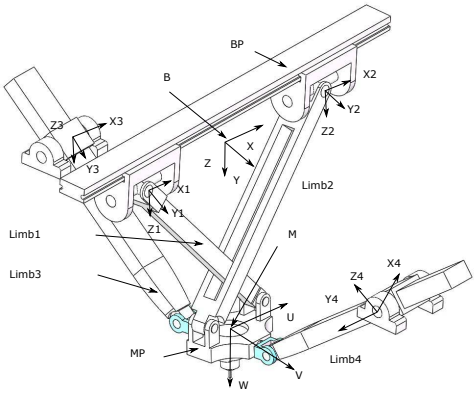

Figure 1: 2PUR-2RPU parallel manipulator

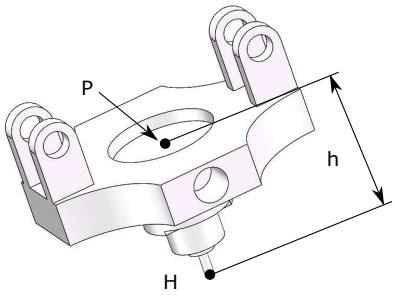

Figure 2: Tool and MP

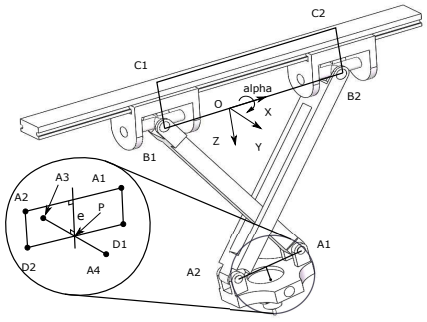

(a) PURRUP chain of limbs 1 & 2

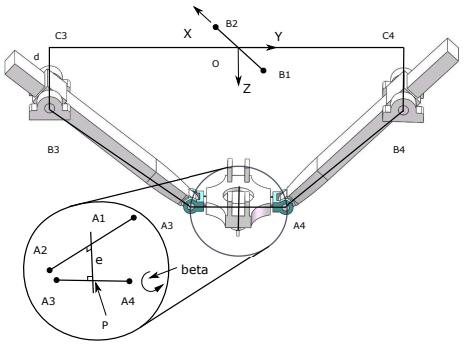

(b) RPUUPR chain of limbs 3 & 4

Figure 3: Dimensions of the 2PUR-2RPU PKM

coordinate frame, $\mathcal{P}(U,V,W)$, is attached to the moving platform at P, the midpoint of the line segment $\overline{A_3A_4}$. Let the X- and the U-axes point in the direction of vectors $\overrightarrow{B_1B_2}$ and $\overrightarrow{A_2A_1}$, respectively. Additionally, a limb-coordinate frame $\mathcal{B}_i(X_i,Y_i,Z_i)$, for $i=1,2,3,4$, is attached to the ith limb at point B_i. When $i=1,2$, the X_i-,Y_i-axes of the limb frames are the revolute axes of the respective U-joints, while the remaining two limb frames define the X_i-axes as the revolute joints, and the Y_i-axes in the direction of $\overrightarrow{B_iA_i}$, respectively.

Let: A_i, for $i=1,2$, denotes a landmark point of each of the two R joints mounted on the MP, as shown in Fig. 3a; for $i=3,4$, A_i denotes the center of each of the two U joints mounted on the MP, as shown in Fig. 3b. As well, B_i, for $i=1,2$, denotes the center of each of the two U joints mounted on the BP; for $i=3,4$, B_i denotes a landmark point of each of the two fixed R joints. Line B_1B_2 is horizontal. Moreover, each C_i, for $i=3,4$, is the intersecting point between the vertical line of B_i and the horizontal plane of line B_1B_2. Thus, one can appreciate that $B_1B_2 \parallel C_1C_2$, $B_3B_4 \parallel C_3C_4$ and $B_1B_2 \perp B_3B_4$. Furthermore, each D_i, for $i=1,2$, is the projection point of A_i onto the U-axis of the frame $\mathcal{P}$. It is noteworthy that C_1 and C_2 are not fixed to the base but move with B_1 and B_2, respectively, along the direction of the corresponding P joint.

2.2. Mobility Analysis

2.2.1. The Displacement Lie-group and its Subgroups

The motion of the moving platform of the PKM of interest is now investigated by means of Lie algebra [35]. A total of 12 displacement subgroups of the group of rigid-body displacements was first identified by Hervé [35] and then applied by Angeles [36] to the qualitative synthesis of parallel manipulators. Four subgroups, of interest to this study, are recalled for quick reference.

1. $\mathcal{R}(\mathcal{A})$, the revolute subgroup of rotations about axis $\mathcal{A}$.
2. $\mathcal{P}(\mathbf{e})$, the prismatic subgroup of translations along the direction of the unit vector $\mathbf{e}$.
3. $\mathcal{F}(\mathbf{w})$, the planar subgroup of one rotation about an axis parallel to the unit vector $\mathbf{w}$ and two independent translations in a plane normal to the same vector.
4. $\mathcal{T}_2(\mathbf{u},\mathbf{v})$, the planar-translation subgroup of translations in the directions of the two distinct unit vectors $\mathbf{u}$ and $\mathbf{v}$.

The definition of *kinematic bond* is recalled here: this is a set of displacements stemming from the product of displacement subgroups [37], while a bond itself need not be a subgroup. Upon using the Lie subgroups for the mobility analysis of parallel manipulators, Li et al. [38] applied the Lie subgroups of displacements to limited-mobility parallel manipulators and obtained an exhaustive enumeration of 3R2T five-dof symmetrical parallel manipulators. Here we recall a list of *mechanical generators* of Lie subgroups of interest to the paper.

1. Mechanical generators of $\mathcal{F}(\mathbf{w})$

(a) $\{\mathcal{R}(A,\mathbf{w}) \bullet \mathcal{R}(B,\mathbf{w}) \bullet \mathcal{R}(C,\mathbf{w})\}$
(b) $\{\mathcal{R}(A,\mathbf{w}) \bullet \mathcal{R}(B,\mathbf{w}) \bullet \mathcal{P}(\mathbf{u})\}$, for $\mathbf{w} \perp \mathbf{u}$

2. Mechanical generators of $\mathcal{T}_2(\mathbf{u},\mathbf{v})$
(a) $\{\mathcal{R}(A,\mathbf{w}) \bullet \mathcal{R}(B,\mathbf{w})\}$, for $\mathbf{w} \perp \mathbf{u},\mathbf{v}$

2.2.2. Mobility Analysis of the 2PUR-2RPU PKM

It is noteworthy that the well-known Chebyshev-Grübler-Kutzbach mobility criterion fails to provide the mobility of the mechanism at hand, which is a *paradoxical chain* in Hervé's classification [39], thereby excluding the possibility of mobility analysis by this criterion. In the three types of kinematic chains proposed by Hervé, only trivial chains can be analyzed by the above-mentioned criterion [39], while the mobility of exceptional and paradoxical chains is to be determined by resorting to other methods. A Lie-group analysis is used instead to investigate the mobility of interest. It is noted that screw theory is another powerful tool to this end, very useful when Lie subgroups cannot be applied.

The motion set of the moving platform in a closed-loop chain is the intersection of the kinematic bonds generated by all the limb-kinematic chains connecting the BP to the MP, i.e.,

$$\mathcal{M} = \bigcap_{i=1}^{n} \{\mathcal{L}_i\} \tag{1}$$

where $\mathcal{M}$ is the motion set of the moving platform, $\mathcal{L}_i$ representing the ith kinematic bond generated by the ith-limb chain, and n the number of limb-chains. Since there are two chains in the manipulator, the PURRUP chain $\mathcal{L}_1$ and the RPUUPR chain $\mathcal{L}_2$, the motion set of the platform can be found as the intersection of the kinematic bonds of these two chains, i.e.,

$$\mathcal{M} = \mathcal{L}_1 \cap \mathcal{L}_2 \tag{2}$$

Similarly, the motion set of each of the two chains can be obtained as the intersection of the two corresponding subchains, i.e.,

$$\mathcal{L}_1 = \mathcal{L}_{11} \cap \mathcal{L}_{12} \tag{3}$$

$$\mathcal{L}_2 = \mathcal{L}_{21} \cap \mathcal{L}_{22} \tag{4}$$

where $\mathcal{L}_1$ is the closed kinematic chain of Fig. 3a, $\mathcal{L}_2$ that of Fig. 3b. Moreover, $\mathcal{L}_{11}$, $\mathcal{L}_{12}$, $\mathcal{L}_{21}$ and $\mathcal{L}_{22}$ are the four bonds of the subchains of limbs 1,2,3,4, respectively, i.e.,

$$\mathcal{L}_{11} = \mathcal{P}(X) \bullet \mathcal{R}(B_1,X) \bullet \mathcal{R}(B_1,V) \bullet \mathcal{R}(A_1,V) \tag{5}$$

$$\mathcal{L}_{12} = \mathcal{P}(X) \bullet \mathcal{R}(B_2,X) \bullet \mathcal{R}(B_2,V) \bullet \mathcal{R}(A_2,V) \tag{6}$$

$$\mathcal{L}_{21} = \mathcal{R}(B_3,X) \bullet \mathcal{P}(\mathbf{e}_1) \bullet \mathcal{R}(A_3,X) \bullet \mathcal{R}(A_3,V) \tag{7}$$

$$\mathcal{L}_{22} = \mathcal{R}(B_4, X) \bullet \mathcal{P}(\mathbf{e}_2) \bullet \mathcal{R}(A_4, X) \bullet \mathcal{R}(A_4, V) \tag{8}$$

It is recalled that the bond product is *idempotent* [37], i.e.,

$$\mathcal{L}(\cdot) \bullet \mathcal{L}(\cdot) = \mathcal{L}(\cdot) \tag{9}$$

Therefore, the motion $\mathcal{M}_i$ generated by the symmetric chains can be identified as

$$\mathcal{L}_1 = \{\mathcal{F}(V) \bullet \mathcal{R}(B_1, X)\} \cap \{\mathcal{F}(V) \bullet \mathcal{R}(B_2, X)\} = \mathcal{F}(V) \bullet \mathcal{R}(X) \tag{10}$$

$$\mathcal{L}_2 = \{\mathcal{F}(X) \bullet \mathcal{R}(A_3, V)\} \cap \{\mathcal{F}(X) \bullet \mathcal{R}(A_4, V)\} = \mathcal{F}(X) \bullet \mathcal{R}(V) \tag{11}$$

Thus, the motion set of the platform $\mathcal{M}$ is given as

$$\begin{aligned} \{\mathcal{M}\} \equiv & \{\mathcal{L}_1\} \cap \{\mathcal{L}_2\} = \{\mathcal{F}(V) \bullet \mathcal{R}(X)\} \cap \{\mathcal{F}(X) \bullet \mathcal{R}(V)\} & (12)\\ = & \{\mathcal{R}(V) \bullet \mathcal{P}(U) \bullet \mathcal{P}(W) \bullet \mathcal{R}(X)\} \cap \{\mathcal{R}(X) \bullet \mathcal{P}(Y) \bullet \mathcal{P}(Z) \bullet \mathcal{R}(V)\} & (13)\\ = & \mathcal{P}(\mathbf{p}) \bullet \mathcal{R}(V) \bullet \mathcal{R}(X) & (14) \end{aligned}$$

This three-degree-of-freedom motion set is not a Lie subgroup, as it lies outside the 12 subgroups in Hervé's classification [39]. The platform is capable of two rotations about corresponding skew axes, X and V, at right angles, and one translation along the vector $\mathbf{p} = \overrightarrow{OP}$, normal to V. It is noteworthy that none of the 12 Lie subgroups identified by Hervé [35] involves two rotation subgroups. We define α, β as the angles of rotation about the X and the V axes, respectively, ζ as the translation along the direction of $\mathbf{p}$.

3. Displacement Analysis

3.1. Inverse-displacement Analysis

When the independent vector of pose variables $\mathbf{x} = [\alpha, \beta, \zeta]^T$ of the moving platform is given, the calculation of vector $\mathbf{q} = [q_1, q_2, q_3, q_4]^T$ of actuated joint variables of $\overline{OB_1}$, $\overline{OB_2}$, $\overline{B_3A_3}$ and $\overline{B_4A_4}$, respectively, called the inverse-displacement solution, is straightforward, as is usual in PKMs. As shown in Fig. 4, the vector-loop equation [2, 40] for the ith link, for $i = 1, 2$, can be written as

$$\mathbf{p} + \mathbf{f}_i + e\mathbf{e}_0 = q_i\mathbf{q}_{i0} + l\mathbf{d}_{i0} \tag{15}$$

where $\mathbf{f}_i = \overrightarrow{PD_i}$, for $i = 1, 2$, while $\mathbf{q}_{i0}$ is the unit vector of the ith actuator displacement. Furthermore, e represents the distance between the two lines A_1A_2 and A_3A_4, while $\mathbf{e}_0$ is the unit vector in the opposite direction of the

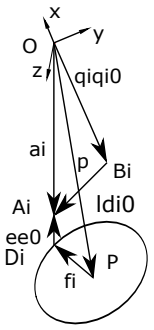

Figure 4: Geometry of one PUR limb

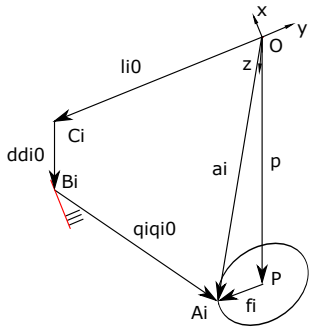

Figure 5: Geometry of one RPU limb

W-axis shown in Fig. 1. Finally, l represents the length of link B_iA_i, and $\mathbf{d}_{i0}$ is a unit vector parallel to $\overrightarrow{B_iA_i}$, for $i = 1, 2$.

Likewise, referring to Fig. 5, for $i = 3, 4$, the vector-loop equation of the RPU link can be obtained as

$$\mathbf{p} + \mathbf{f}_i = l_i\mathbf{l}_{i0} + d\mathbf{d}_{i0} + q_i\mathbf{q}_{i0} \tag{16}$$

where $\mathbf{f}_i = \overrightarrow{PA_i}$, for $i = 3, 4$, while l_i represents the magnitude of $\overrightarrow{OC_i}$, and $\mathbf{l}_{i0}$ is the unit vector in the direction of $\overrightarrow{OC_i}$, for $i = 3, 4$. Moreover, $\mathbf{d}_{i0}$ is a unit vector parallel to $\overrightarrow{C_iB_i}$, and d the length of C_iB_i, for $i = 3, 4$.

Upon taking the norm of both sides of Eq. (15) and rearranging terms, while considering that $\mathbf{f}_i \perp \mathbf{e}_0$, we obtain

$$q_i^2 + 2\mathbf{q}_{i0}^T\mathbf{d}_{i0}lq_i + l^2 - \zeta^2 - f_i^2 - e^2 - 2\mathbf{p}^T\mathbf{f}_i - 2e\mathbf{p}^T\mathbf{e}_0 = 0, \quad i = 1, 2 \tag{17}$$

Hence, the inverse-kinematics solutions are obtained as

$$q_i = -\mathbf{q}_{i0}^T\mathbf{d}_{i0}l \pm \sqrt{\left(\mathbf{q}_{i0}^T\mathbf{d}_{i0}l\right)^2 + \zeta^2 + f_i^2 + e^2 - l^2 + 2\mathbf{p}^T\mathbf{f}_i + 2e\mathbf{p}^T\mathbf{e}_0}, \quad i = 1, 2 \tag{18}$$

Similarly, upon taking the norm of both sides of Eq. (16) and rearranging terms, while considering that $\mathbf{p} \perp \mathbf{f}_i$ for $i = 3, 4$, we obtain

$$q_i^2 + 2\mathbf{q}_{i0}^T(l_i\mathbf{l}_{i0} + d\mathbf{d}_{i0})q_i + l_i^2 + d^2 - \zeta^2 - f_i^2 = 0, \quad i = 3, 4 \tag{19}$$

Therefore,

$$q_i = -\mathbf{q}_{i0}^T(l_i\mathbf{l}_{i0} + d\mathbf{d}_{i0}) \pm \sqrt{\left(\mathbf{q}_{i0}^T(l_i\mathbf{l}_{i0} + d\mathbf{d}_{i0})\right)^2 + \zeta^2 + f_i^2 - l_i^2 - d^2}, \quad i = 3, 4 \tag{20}$$

thereby obtaining two solutions per actuator. Hence, $2^4 = 16$ inverse-kinematics solutions for a given platform pose are possible.

We investigate next the solution of the inverse-displacement problem. Let the position vector of point A_i, for $i = 1, 2, 3, 4$, expressed in frames $\mathcal{B}$ and $\mathcal{P}$, be denoted by $[\mathbf{a}_i]_{\mathcal{B}}$ and $[\mathbf{a}_i]_{\mathcal{P}}$, respectively. Furthermore, the rotation matrix from $\mathcal{P}$ to $\mathcal{B}$ is represented by $[\mathbf{Q}]_{\mathcal{B}}$, the subscript of the brackets identifying the coordinate frame in which a vector or a matrix is expressed. For brevity, the subscript will be omitted whenever the coordinate frame is the fixed frame $\mathcal{B}$. The matrix rotating frame $\mathcal{B}$ to frame $\mathcal{P}$ is calculated below:

$$\mathbf{Q} = \mathbf{Q}_x(\alpha)\mathbf{Q}_y(\beta) = \begin{bmatrix} 1 & 0 & 0 \\ 0 & \cos\alpha & -\sin\alpha \\ 0 & \sin\alpha & \cos\alpha \end{bmatrix} \begin{bmatrix} \cos\beta & 0 & \sin\beta \\ 0 & 1 & 0 \\ -\sin\beta & 0 & \cos\beta \end{bmatrix} \tag{21}$$

$$= \begin{bmatrix} \cos\beta & 0 & \sin\beta \\ \sin\alpha\sin\beta & \cos\alpha & -\sin\alpha\cos\beta \\ -\cos\alpha\sin\beta & \sin\alpha & \cos\alpha\cos\beta \end{bmatrix} \tag{22}$$

Moreover, we have

$$\mathbf{a}_i = \mathbf{Q}_{\mathcal{P}}[\mathbf{a}_i]_{\mathcal{P}} + \mathbf{p}, \qquad \text{for} \quad i = 1, 2, 3, 4 \tag{23}$$

and

$$[\mathbf{a}_1]_{\mathcal{P}} = [f_1 \quad 0 \quad -e]^T,\ [\mathbf{a}_2]_{\mathcal{P}} = [-f_1 \quad 0 \quad -e]^T \tag{24a}$$

$$[\mathbf{a}_3]_{\mathcal{P}} = [0 \quad -f_3 \quad 0]^T,\ [\mathbf{a}_4]_{\mathcal{P}} = [0 \quad f_3 \quad 0]^T \tag{24b}$$

where f_i is the magnitude of $\mathbf{f}_i$; and $\mathbf{p} = [0 \quad -\zeta\sin\alpha \quad \zeta\cos\alpha]^T$ denotes the position vector of point P. Let θ_i denote the angle between Z_i and $\overrightarrow{B_iA_i}$ for $i = 1, 2$, and between Y_i and Y for $i = 3, 4$. Moreover, $\mathbf{a}_i$ can be obtained through another rotation matrix $\mathbf{Q}_i$ that represents the rotation from frame $\mathcal{B}$ to frame $\mathcal{B}_i$, thus obtaining

$$\mathbf{a}_i = \mathbf{Q}_i[\mathbf{a}_i]_{\mathcal{B}i} + \mathbf{b}_i, \quad \text{for} \quad i = 1, 2, 3, 4 \tag{25}$$

with

$$\mathbf{Q}_1 = \mathbf{Q}_2 = \mathbf{Q}_x(\alpha) = \begin{bmatrix} 1 & 0 & 0 \\ 0 & \cos\alpha & -\sin\alpha \\ 0 & \sin\alpha & \cos\alpha \end{bmatrix} \tag{26a}$$

$$\mathbf{Q}_3 = \mathbf{Q}_x(\theta_3) = \begin{bmatrix} 1 & 0 & 0 \\ 0 & \cos\theta_3 & -\sin\theta_3 \\ 0 & \sin\theta_3 & \cos\theta_3 \end{bmatrix} \tag{26b}$$

$$\mathbf{Q}_4 = \mathbf{Q}_x(\theta_4) = \begin{bmatrix} 1 & 0 & 0 \\ 0 & \cos\theta_4 & -\sin\theta_4 \\ 0 & \sin\theta_4 & \cos\theta_4 \end{bmatrix} \tag{26c}$$

where the origin B_i of the respective limb frame, expressed in $\mathcal{B}$, is obtained as

$$\mathbf{b}_1 = [q_1 \quad 0 \quad 0]^T,\ \mathbf{b}_2 = [q_2 \quad 0 \quad 0]^T,\ \mathbf{b}_3 = [0 \quad -l_3 \quad d]^T,\ \mathbf{b}_4 = [0 \quad l_3 \quad d]^T \tag{27}$$

and the position vector of point A_i, $[\mathbf{a}_i]_{\mathcal{B}i}$, expressed in $\mathcal{B}_i$, for $i = 1, 2, 3, 4$, is given by

$$[\mathbf{a}_1]_{\mathcal{B}1} = [l\sin\theta_1 \quad 0 \quad l\cos\theta_1]^T,\ [\mathbf{a}_2]_{\mathcal{B}2} = [-l\sin\theta_2 \quad 0 \quad l\cos\theta_2]^T \tag{28a}$$

$$[\mathbf{a}_3]_{\mathcal{B}3} = [0 \quad q_3 \quad 0]^T,\ [\mathbf{a}_4]_{\mathcal{B}4} = [0 \quad q_4 \quad 0]^T \tag{28b}$$

Upon recalling Eqs. (23) and (25), and denoting the same position vectors of points A_i in the frame $\mathcal{B}$ through different paths, we substitute the right-hand sides of these two equations with their corresponding entries, thus obtaining

$$l\sin\theta_1 + q_1 = f_1\cos\beta - e\sin\beta \tag{29a}$$

$$l\cos\theta_1 = \zeta - f_1\sin\beta - e\cos\beta \tag{29b}$$

$$q_2 - l\sin\theta_2 = -f_1\cos\beta - e\sin\beta \tag{29c}$$

$$l\cos\theta_2 = \zeta + f_1\sin\beta - e\cos\beta \tag{29d}$$

$$q_3\cos\theta_3 - l_3 = -f_3\cos\alpha - \zeta\sin\alpha \tag{29e}$$

$$q_3\sin\theta_3 + d = -f_3\sin\alpha + \zeta\cos\alpha \tag{29f}$$

$$q_4\cos\theta_4 + l_3 = f_3\cos\alpha - \zeta\sin\alpha \tag{29g}$$

$$q_4\sin\theta_4 + d = f_3\sin\alpha + \zeta\cos\alpha \tag{29h}$$

Now let

$$g_{11} = l\sin\theta_1, \quad g_{12} = l\cos\theta_1 \tag{30a}$$

$$g_{21} = l\sin\theta_2, \quad g_{22} = l\cos\theta_2 \tag{30b}$$

$$g_{31} = q_3\sin\theta_3, \quad g_{32} = q_3\cos\theta_3 \tag{30c}$$

$$g_{41} = q_4\sin\theta_4, \quad g_{42} = q_4\cos\theta_4 \tag{30d}$$

Upon substitution of expressions (30a) through (30d) into Eqs. (29a) through (29h), g_{ij} can be obtained as

$$g_{11} = \sqrt{l^2 - (\zeta - f_1\sin\beta - e\cos\beta)^2}, \quad g_{12} = \zeta - f_1\sin\beta - e\cos\beta \tag{31a}$$

$$g_{21} = \sqrt{l^2 - (\zeta + f_1\sin\beta - e\cos\beta)^2}, \quad g_{22} = \zeta + f_1\sin\beta - e\cos\beta \tag{31b}$$

$$g_{31} = \zeta\cos\alpha - f_3\sin\alpha - d, \quad g_{32} = l_3 - f_3\cos\alpha - \zeta\sin\alpha \tag{31c}$$

$$g_{41} = \zeta\cos\alpha + f_3\sin\alpha - d, \quad g_{42} = -l_3 + f_3\cos\alpha - \zeta\sin\alpha \tag{31d}$$

Hence, the unique inverse-displacement solution for the 2PUR-2PUR PKM is obtained as

$$\mathbf{q} = \begin{bmatrix} -g_{11} + f_1\cos\beta - e\sin\beta \\ g_{21} - f_1\cos\beta - e\sin\beta \\ \sqrt{g_{31}^2 + g_{32}^2} \\ \sqrt{g_{41}^2 + g_{42}^2} \end{bmatrix} \tag{32}$$

3.2. Direct-displacement Analysis

First, Eq. (32) leads to

$$g_{11} = f_1\cos\beta - e\sin\beta - q_1,\ g_{21} = f_1\cos\beta + e\sin\beta + q_2 \tag{33a}$$

$$q_3 = \sqrt{g_{31}^2 + g_{32}^2},\ q_4 = \sqrt{g_{41}^2 + g_{42}^2} \tag{33b}$$

Substituting g_{ij} from Eqs. (31a) to (31d) into Eq. (33), then squaring both sides of these equations yields

$$\zeta^2 + 2(q_1 e - f_1\zeta)\sin\beta - 2(f_1 q_1 + \zeta e)\cos\beta + e^2 + f_1^2 + q_1^2 - l^2 = 0 \tag{34a}$$

$$\zeta^2 + 2(q_2 e + f_1\zeta)\sin\beta + 2(f_1 q_2 - \zeta e)\cos\beta - e^2 + f_1^2 + q_2^2 - l^2 = 0 \tag{34b}$$

$$\zeta^2 - 2(l_3 f_3 + \zeta d)\cos\alpha + 2(df_3 - l_3\zeta)\sin\alpha + d^2 + l_3^2 + f_3^2 - q_3^2 = 0 \tag{34c}$$

$$\zeta^2 - 2(l_3 f_3 + \zeta d)\cos\alpha - 2(df_3 - l_3\zeta)\sin\alpha + d^2 + l_3^2 + f_3^2 - q_4^2 = 0 \tag{34d}$$

Upon adding sidewise Eqs. (34a) and (34b), then subtracting the former from the latter, next proceeding likewise with Eqs. (34c) and (34d), we obtain

$$\zeta^2 + 2e\zeta\cos\beta + \lambda_1\cos\beta + \lambda_3\sin\beta + \lambda_5 = 0 \tag{35a}$$

$$2f_1\zeta\sin\beta + \lambda_2\cos\beta + \lambda_4\sin\beta + \lambda_6 = 0 \tag{35b}$$

$$\zeta^2 - 2\mu_2\cos\alpha - 2d\zeta\cos\alpha + \mu_3 = 0 \tag{35c}$$

$$(\mu_1 - l_3\zeta)\sin\alpha + \mu_4 = 0 \tag{35d}$$

where

$$\lambda_1 = f_1(q_2 - q_1), \quad \lambda_2 = f_1(q_2 + q_1), \quad \lambda_3 = e(q_2 + q_1) \tag{36a}$$

$$\lambda_4 = e(q_2 - q_1), \quad \lambda_5 = \frac{q_1^2 + q_2^2}{2} + f_1^2 - l^2, \quad \lambda_6 = \frac{q_2^2 - q_1^2}{2} - e^2 \tag{36b}$$

$$\mu_1 = df_3, \quad \mu_2 = l_3 f_3 \tag{36c}$$

$$\mu_3 = -\frac{q_3^2 + q_4^2}{2} + f_3^2 + d^2 + l_3^2 \quad \mu_4 = \frac{q_4^2 - q_3^2}{4} \tag{36d}$$

Equations (35c & 35d) yield

$$\cos\alpha = \frac{\zeta^2 + \mu_3}{2(\mu_2 + d\zeta)}, \quad \sin\alpha = \frac{\mu_4}{l_3\zeta - \mu_1} \tag{37}$$

Upon squaring both sides of Eq. (37), then adding them sidewise yields

$$\frac{(\zeta^2 + \mu_3)^2}{4(\mu_2 + d\zeta)^2} + \frac{\mu_4^2}{(l_3\zeta - \mu_1)^2} = 1 \tag{38}$$

From the foregoing equation we obtain a sixth-degree polynomial in ζ:

$$\nu_0\zeta^6 + \nu_1\zeta^5 + \nu_2\zeta^4 + \nu_3\zeta^3 + \nu_4\zeta^2 + \nu_5\zeta + \nu_6 = 0 \tag{39}$$

where ν_i, $i = 0, 1, \cdots, 6$, is a function of the geometric parameters of the mechanism and its joint coordinates. Once ζ is known, Eq. (37) yields one single value for α, while Eqs. (35a) and (35b) yield one single value for β. It can be concluded that the direct-kinematics of the moving platform admits six MP poses, some feasible, some unfeasible, depending on the nature of the roots of Eq. (39), some real, some complex. However, it is cumbersome to derive all possible configurations of the moving platform through this approach. Hence, for the purpose of control, a numerical method is recommended to solve the direct-displacement problem.

4. Velocity Analysis

4.1. Vector Loop-Equation

Differentiation of both sides of Eq. (15) with respect to time yields

$$\mathbf{v}_P + \boldsymbol{\omega}_\mathcal{P} \times \mathbf{f}_i + e\boldsymbol{\omega}_\mathcal{P} \times \mathbf{e}_0 = \dot{q}_i\mathbf{q}_{i0} + l\boldsymbol{\omega}_i \times \mathbf{d}_{i0} \quad \text{for} \quad i = 1, 2 \tag{40}$$

Upon dot-multiplying both sides of Eq. (40) by $\mathbf{d}_{i0}$ to eliminate the passive variable $\boldsymbol{\omega}_i$, we obtain

$$\mathbf{v}_P^T\mathbf{d}_{i0} + (\boldsymbol{\omega}_\mathcal{P} \times \mathbf{f}_i)^T\mathbf{d}_{i0} + e(\boldsymbol{\omega}_\mathcal{P} \times \mathbf{e}_0)^T\mathbf{d}_{i0} = \dot{q}_i\mathbf{q}_{i0}^T\mathbf{d}_{i0} \tag{41}$$

which, after rearranging, becomes

$$\mathbf{d}_{i0}^T\mathbf{v}_P + (\mathbf{f}_i \times \mathbf{d}_{i0})^T\boldsymbol{\omega}_\mathcal{P} + (e\mathbf{e}_0 \times \mathbf{d}_{i0})^T\boldsymbol{\omega}_\mathcal{P} = \dot{q}_i\mathbf{d}_{i0}^T\mathbf{q}_{i0} \tag{42}$$

Similarly, differentiation of both sides of Eq. (16) with respect to time yields

$$\mathbf{v}_P + \boldsymbol{\omega}_\mathcal{P} \times \mathbf{f}_i = q_i\boldsymbol{\omega}_i \times \mathbf{q}_{i0} + \dot{q}_i\mathbf{q}_{i0} \quad \text{for} \quad i = 3, 4 \tag{43}$$

Then, upon dot-multiplying both sides of Eq. (43) by $\mathbf{q}_{i0}$, we obtain

$$\mathbf{v}_P^T\mathbf{q}_{i0} + (\boldsymbol{\omega}_\mathcal{P} \times \mathbf{f}_i)^T\mathbf{q}_{i0} = \dot{q}_i \tag{44}$$

which, likewise, upon rearranging, becomes

$$\mathbf{q}_{i0}^T\mathbf{v}_P + (\mathbf{f}_i \times \mathbf{q}_{i0})^T\boldsymbol{\omega}_\mathcal{P} = \dot{q}_i \tag{45}$$

Now, $\mathbf{t}_{\mathcal{P}} = [\mathbf{v}_P^T \quad \boldsymbol{\omega}_{\mathcal{P}}^T]^T$ denotes the twist of the moving platform, while keeping in mind that only three of its six components are independent. We obtain, after straightforward manipulations,

$$\mathbf{K}_p \mathbf{t}_{\mathcal{P}} = \mathbf{J}_q \dot{\mathbf{q}} \tag{46}$$

where

$$\mathbf{J}_q = \begin{bmatrix} \mathbf{d}_{10}^T \mathbf{q}_{10} & 0 & 0 & 0 \\ 0 & \mathbf{d}_{20}^T \mathbf{q}_{20} & 0 & 0 \\ 0 & 0 & 1 & 0 \\ 0 & 0 & 0 & 1 \end{bmatrix}, \quad \mathbf{K}_p = \begin{bmatrix} \mathbf{d}_{10}^T & (\mathbf{f}_1 \times \mathbf{d}_{10})^T + e(\mathbf{e}_0 \times \mathbf{d}_{10})^T \\ \mathbf{d}_{20}^T & (\mathbf{f}_2 \times \mathbf{d}_{20})^T + e(\mathbf{e}_0 \times \mathbf{d}_{20})^T \\ \mathbf{q}_{30}^T & (\mathbf{f}_3 \times \mathbf{q}_{30})^T \\ \mathbf{q}_{40}^T & (\mathbf{f}_4 \times \mathbf{q}_{40})^T \end{bmatrix} \tag{47}$$

4.2. Velocity Equation

Differentiation of both sides of Eq. (32) with respect to time yields

$$\mathbf{J}_r \dot{\mathbf{q}} = \mathbf{K} \mathbf{t} \tag{48}$$

where $\mathbf{t} \equiv [\dot{\alpha} \ \dot{\beta} \ \dot{\zeta}]^T$ denotes the three-dimensional twist of the MP, composed of the two independent angular speeds $\dot{\alpha}$ and $\dot{\beta}$, along with the speed $\dot{\zeta}$. Furthermore,

$$\mathbf{J}_r = \begin{bmatrix} J_{11} & 0 & 0 & 0 \\ 0 & J_{22} & 0 & 0 \\ 0 & 0 & J_{33} & 0 \\ 0 & 0 & 0 & J_{44} \end{bmatrix}, \qquad \mathbf{K} = \begin{bmatrix} 0 & K_{11} & K_{13} \\ 0 & K_{21} & K_{23} \\ K_{32} & 0 & K_{33} \\ K_{42} & 0 & K_{43} \end{bmatrix} \tag{49}$$

with

$$\begin{aligned}
J_{11} =& g_{11}, \quad J_{22} = g_{21}, \quad J_{33} = \sqrt{g_{31}^2 + g_{32}^2}, \quad J_{44} = \sqrt{g_{41}^2 + g_{42}^2} \\
K_{11} =& -g_{11} f_1 \sin\beta - g_{11} e \cos\beta + (\zeta - f_1 \sin\beta - e\cos\beta)(e\sin\beta - f_1 \cos\beta) \\
K_{21} =& g_{21} f_1 \sin\beta - g_{21} e \cos\beta - (\zeta + f_1 \sin\beta - e\cos\beta)(f_1 \cos\beta + e \sin\beta) \\
K_{13} =& \zeta - f_1 \sin\beta - e\cos\beta, \quad K_{23} = -f_1 \sin\beta - \zeta + e\cos\beta \\
K_{32} =& -g_{31}(\zeta \sin\alpha + f_3 \cos\alpha) + g_{32}(f_3 \sin\alpha - \zeta \cos\alpha) \\
K_{33} =& g_{31} \cos\alpha - g_{32} \sin\alpha \\
K_{42} =& g_{41}(-\zeta \sin\alpha + f_3 \cos\alpha) - g_{42}(f_3 \sin\alpha + \zeta \cos\alpha) \\
K_{43} =& g_{41} \cos\alpha - g_{42} \sin\alpha
\end{aligned}$$

5. Singularity Analysis

When any of the two Jacobian matrices becomes either singular or rank-deficient, as the case may be, the mechanism finds itself at a singularity, as explained

below. At a singular configuration, the system loses either stiffness or mobility, thereby falling into either uncontrollable motion or deficient performance. From a result on the singularity analysis of PKMs [41], the singularity problem of general closed-loop kinematic chains, such as PKMs, can be divided into three types: Type-I, direct-kinematics singularity; Type-II, inverse-kinematics singularity; and Type-III, combined singularity. Besides the aforementioned singularities, there may exist other types in constrained PKMs, namely, *constraint-singularities* [42], which cannot be identified by the rank-deficiency of the Jacobian matrices. At such singularities, the constraint wrenches degenerate, thereby increasing instantaneously the degree of freedom of the MP. Thus, it is essential to look for constraint singularities before eliminating the passive velocities.

Recalling Eq. (46) and considering the rank deficiency of the matrices concerned, the three types of singularity are now identified, while constraint-singularity is analyzed by resorting to constraint wrenches.

5.1. Type-I: Direct-kinematics Singularity

A singularity of this type occurs when the 4×6 $\mathbf{K}_p$ matrix is rank-deficient. In order to characterize the rank-deficiency of interest, let

$$\mathbf{n}_i = \begin{cases} (\mathbf{f}_i + e\mathbf{e}_0) \times \mathbf{d}_{i0}, & \text{if} \quad i = 1, 2 \\ \mathbf{f}_i \times \mathbf{q}_{i0}, & \text{if} \quad i = 3, 4 \end{cases} \tag{51}$$

Vector $\mathbf{n}_i$ is normal to the plane defined by points P, A_i, and B_i. One can readily notice that $\mathbf{n}_1$ and $\mathbf{n}_2$ are parallel, while $\mathbf{n}_3$ is parallel to $\mathbf{n}_4$. However, the foregoing linear-dependency does not lead to the rank-deficiency of $\mathbf{K}_p$. If two or more of the vectors of $\mathbf{K}_p$ vanish, then the matrix is rank-deficient. Indeed, let us assume that

$$\mathbf{n}_i = \mathbf{0}, \quad \text{for } i \in \{1, 2\} \quad \text{and} \quad \mathbf{n}_j = 0, \quad \text{for } j \in \{3, 4\} \tag{52}$$

which means that (i) line A_iB_i coincides with line PA_i, for the $\underline{\text{P}}$URRU$\underline{\text{P}}$ chain, when $i = 1, 2$ and (ii) A_iB_i coincides with the V-axis of the moving frame $\mathcal{P}$, for the R$\underline{\text{P}}$UU$\underline{\text{P}}$R chain, when $i = 3, 4$. It is noteworthy, however, that only the condition for $i = 3, 4$ is possible, as A_1B_1 and A_2B_2 cannot coincide with lines PA_1 and PA_2, respectively, because of interference. As a result, the mechanism acquires one or more degrees of freedom in the presence of this singularity, even when all the actuators are locked.

5.2. Type-II: Inverse-kinematics Singularity

On the other hand, the mechanism finds itself at an inverse-kinematics singular posture when $\mathbf{J}_q$ is singular. The determinant of the diagonal matrix $\mathbf{J}_q$ of Eq. (47) vanishes if at least one of its first two diagonal entries does, i.e., if

$$\mathbf{d}_{i0}^T \mathbf{q}_{i0} = 0, \quad \text{for} \quad i \in \{1, 2\} \tag{53}$$

Under the above singularity, $OB_i \perp B_iA_i$. The perpendicularity of these two lines leads to a posture under which the axis of at least one of the legs is perpendicular to its actuator direction, the mechanism thus losing one or two degrees of freedom instantaneously, depending on the number of perpendicularity cases. This type of singularity, however, will not occur in the mechanism at hand because of the geometric constraints imposed by the link shapes of the two cross links, B_1A_1 and B_2A_2, by design.

5.3. Type-III: Combined Singularity

The combined singularity occurs when both $\mathbf{K}_p$ and $\mathbf{J}_q$ are rank-deficient simultaneously. Since the second singularity is precluded by the geometry of the robot, this third type of singularity is also precluded.

5.4. Constraint-Singularity

From the viewpoint of constraints, a kinematic chain with reduced mobility experiences internal constraint wrenches. The two limb chains, of four-dof, exert one constraint on the three-dof MP. We define $\mathbf{p}_\perp$ as a unit vector that is perpendicular to $\mathbf{p}$ in the plane spanned by lines A_1B_1 and A_2B_2. When $\mathbf{p}_\perp$ is parallel to V, this constraint vanishes, and the MP, as a result, finds itself at a posture of four dof instantaneously. Thus, Eq. (12) has the form:

$$\{\mathcal{M}\} \equiv \{\mathcal{L}_1\} \cap \{\mathcal{L}_2\} = \{\mathcal{F}(V) \bullet \mathcal{R}(X)\} \cap \{\mathcal{F}(X) \bullet \mathcal{R}(V)\} \tag{54}$$

$$= \{\mathcal{R}(V) \bullet \mathcal{P}(\mathbf{p}) \bullet \mathcal{P}(\mathbf{p}_\perp) \bullet \mathcal{R}(X)\} \cap \{\mathcal{R}(X) \bullet \mathcal{P}(\mathbf{p}) \bullet \mathcal{P}(V) \bullet \mathcal{R}(V)\} \tag{55}$$

$$= \mathcal{F}(V) \bullet \mathcal{R}(X) \tag{56}$$

This means that the two-limb chains have the same constraints on the MP. Under these constraints, the MP can undergo two independent translations and two independent rotations. This type of singularities, however, will never occur in the robot because of the geometric constraints imposed, ensuring that $\mathbf{p}_\perp$ cannot be parallel to V.

6. Workspace Analysis

6.1. Physical Constraints and Algorithms

The reachable workspace of a PKM is defined as the set of points that can be reached by the operation point in the moving platform, and the set of orientations attained by the MP [2]. The concept is essential to determining the workspace boundaries, its singularities and voids, for the design and performance analysis of a manipulator [43]. Compared with their serial counterparts, PKMs have relatively small workspaces. Therefore, the workspace of PKMs is an important concept that reflects their performance.

Point P, located at the center of the moving platform, is the reference point and can only move in the plane spanned by lines A_3B_3 and A_4B_4. An axially symmetric tool, with its axis passing through P, as shown in Fig. 2, is to be

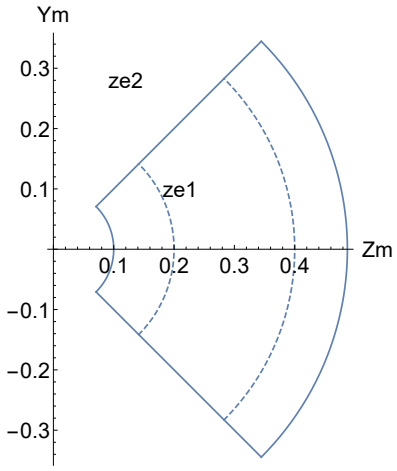

(a) workspace of the reference point P

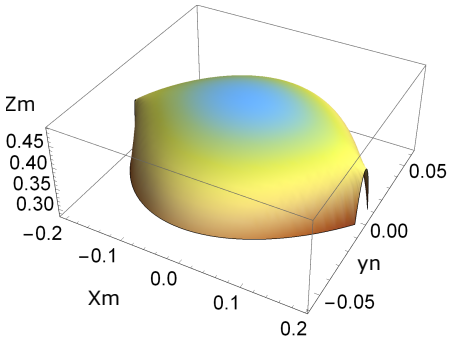

(b) subdomain of workspace of the tool head H in case of $\zeta = 0.2$ m

Figure 6: Reachable workspace of a 2PUR-2RPU PKM

added, as the need arises. Hence, the workspace problem of the robot can be significantly simplified by investigating the workspace of P first. We can arbitrarily set β to be 0 because it does not affect the computation of the robot workspace with respect to the reference point P. By varying the remaining coordinates, α and ζ, one can readily prove that the workspace "volume"[3] V is given by

$$V = \int_{\zeta_{\min}}^{\zeta_{\max}} \zeta \Delta\alpha d\zeta \tag{57}$$

which, in this case, lies in a plane; V is the area reachable by the said point P. Considering the architecture constraints of the manipulator, $\zeta_{\max}$ and $\zeta_{\min}$ denote the maximum and the minimum distance between P and O, $\Delta\alpha$ being the range of orientation of α. We assume that the motion range of each prismatic actuator is within ± 0.2 m, and its rotational range of motion is set as $\pm\pi/4$.

6.2. Case Studies

The architectural parameters of the manipulator are selected as $l = 0.6$ m, $l_3 = 0.4$ m, $f_i = 0.3$ m (for $i = 1, 3$), $d = 0.1$ m and $e = 0$ m. Upon considering the physical constraints of the joints, we let $\zeta_{min} = 0.1$ m. Next we calculate the range of ζ to obtain the reachable workspace of the manipulator. One can readily show that the position of the largest ζ is reached when the two U-joints of the PURRUP chain find themselves closest to the origin O. The

[3]Quotation marks intended to acknowledge that, rather than a three-dimensional volume, what we have is a two-dimensional region.

two U-joints, however, cannot reach the said origin because of the physical constraints imposed by themselves. We assume a limit $q_{\min} = 0.05$ m for q_3 and q_4. Therefore,

$$\zeta_{\max} = \sqrt{l^2 - \left(\frac{f_3 + f_4 + 2q_{\min}}{2}\right)^2} \approx 0.4873 \text{ m} \tag{58}$$

Upon recalling Eq. (57) one can readily find $V = 0.1787$ m^2. Furthermore, since a tool is added at the point P in machining applications, the workspace of the tool head is three-dimensional, as depicted in Fig. 6b, where the optimum length of the tool is 0.2874 m, as derived from condition-number minimization in Subsection 7.2. It is pointed out that, although the workspace of the tool head lies in three-dimensional space, its dof is two rotations plus one translation, obtained by fixing the length of the translational displacement ζ, then rotating the MP around two axes X and V with feasible α and β. With varied length of ζ, the reachable workspace of the tool head is obtained by the aforementioned geometrical approach.

7. Dexterity Analysis

7.1. Dexterity Indices

It is of the utmost importance to establish and quantify the different performance characteristics of a mechanism. As most kinematic performance measures are based on the Jacobian, and its invariants, such as determinant, eigenvalues, singular values, and condition number, it is an indispensable matrix in understanding the motion of the end-effector [44]. Performance indices such as manipulability, defined as the square root of the determinant of $\mathbf{JJ}^T$ [45], and the condition number of the Jacobian matrix [46] are well known. The Jacobian $\mathbf{J}$ of interest is defined as:

$$\mathbf{J} = \mathbf{J}_r^{-1}\mathbf{K} \tag{59}$$

The foregoing 4×3 Jacobian $\mathbf{J}$ is the result of actuation-redundancy, namely, the use of four actuators to control three independent pose variables.

Since, in general, a Jacobian matrix is configuration-dependent, the above-mentioned metrics are local performance indices that give an indication of how far the manipulator posture is from a singularity. It is noteworthy that, in fact, the determinant of a square matrix tells only if and when a matrix is invertible, but it does not tell the *invertibility* of the matrix [33]. The maximum-singular-value based sensitivity indices [47] suffer from a significant limitations, as they are scale-dependent. Hence, we investigate the numerical properties of the Jacobian matrix using the condition number, rather than the manipulability and the sensitivity.

A posture-independent index, termed the *kinetostatic conditioning index* (KCI), introduced elsewhere [33], is given by

$$\mathrm{KCI} = \frac{1}{\kappa_{\min}} \times 100\% \tag{60}$$

Since the condition number is bounded from below, the KCI is bounded from above by a value of 100%. Manipulators with a KCI of 100%, those with a minimum condition number of 1.0, are termed *isotropic*, which is one of the objectives of design optimization.

In general, any Jacobian matrix includes both dimensionless entries and entries with units of length, which prevents the computation of the condition number [48]. To cope with this challenge, a dimensionally homogeneous Jacobian, $\mathbf{J}_h$, was proposed [33] by means of the concept of *characteristic length*. A performance index, termed the *global conditioning index* (GCI), was introduced to represent the dexterity over the entire workspace, rather than at a certain posture [49]. The GCI is defined as

$$\mathrm{GCI} = \frac{\int_{\mathcal{W}} (1/\kappa) dV}{V} \tag{61}$$

where V is the volume of the workspace, $\mathcal{W}$ is the entire robot workspace and κ is the condition number at a particular point of $\mathcal{W}$.

It is pointed out, however, that several other approaches are available to cope with the limitations of scale dependence and inhomogeneity, inherent in the Jacobian based metrics. A formulation for the kinematic equations, using the velocity of some points of the end-effector, rather than only one point in it, thus leading to homogeneous Cartesian rates, was proposed by Gosselin [50]. However, this formulation requires that all joints be of the same type. Thus, kinematic-sensitivity indices for dimensionally inhomogeneous Jacobian matrices, namely, the *maximum rotation sensitivity* and the *maximum point-displacement sensitivity*, were introduced as two distinct metrics with a clear physical meaning [51]. Although this is an alternative approach to dexterity analysis, it entails a significant drawback, namely, being applicable only to uniformly actuated manipulators.

Other metrics, not based on the Jacobian, such as *motion/force transmission index*[52] and *power manipulability* [53], lie outside the scope of this paper. The former is based on the power coefficient to evaluate the motion/force transmissibility from a wrench to a twist, while the latter concerns the study of power within the mechanism.

7.2. Condition-number Minimization

The condition number κ of a matrix $\mathbf{J}$, our Jacobian, is defined as [54]:

$$\kappa = \|\mathbf{J}\| \|\mathbf{J}^{-1}\| \tag{62}$$

where $\|\cdot\|$ denotes any norm of its matrix argument. Note that the Frobenius norm is frame-invariant and analytic, i.e., it admits infinitely many derivatives w.r.t. it, gradient methods thus being applicable to minimizing the condition number over architecture parameters and posture variables. Therefore, the Frobenius norm is used throughout this paper. Moreover, we use the homogeneous Jacobian, $\mathbf{J}_h$, instead of the raw Jacobian, $\mathbf{J}$, to allow for the computation of the condition number κ, and hence,

$$\kappa = \|\mathbf{J}_h\|\|{\mathbf{J}_h}^{-1}\| \tag{63}$$

where $\mathbf{J}_h$ is obtained upon normalization of $\mathbf{J}$ [33], namely,

$$\mathbf{J}_h = \mathbf{J}\,\mathrm{diag}(\frac{1}{L} \quad \frac{1}{L} \quad 1) \tag{64}$$

where L is the characteristic length, to be determined in the sequel. Of course, this normalization calls for a redefinition of the kinematic variables, Cartesian or joint coordinates, to ensure that the kinematic relations are preserved. It is noteworthy that PKMs usually involve two Jacobians, namely, the forward Jacobian $\mathbf{K}$ and the inverse Jacobian $\mathbf{J}_r$. The inverse Jacobian $\mathbf{J}_r$ is dimensionally homogeneous because all four actuators are of the same class, namely, prismatic joints. For the purpose of rendering the forward Jacobian matrix $\mathbf{K}$ dimensionally homogeneous, we redefine it in the form [33]

$$\mathbf{K} = [\mathbf{K}_p \quad \mathbf{k}_o] \tag{65}$$

where the 4×2 matrix $\mathbf{K}_p$ is the position sub-Jacobian and the four-dimensional vector array $\mathbf{k}_o$ the orientation sub-Jacobian. Hence, the homogeneous forward Jacobian takes the form

$$\mathbf{K}_h = [\frac{1}{L}\mathbf{K}_p \quad \mathbf{k}_o] \tag{66}$$

Thus, the isotropy condition for $\mathbf{K}_h$ is

$${\mathbf{K}_h}^T\mathbf{K}_h = \begin{bmatrix} \frac{1}{L^2}\mathbf{K}_p^T\mathbf{K}_p & \frac{1}{L}\mathbf{K}_p^T\mathbf{k}_o \\ \frac{1}{L}\mathbf{k}_o^T\mathbf{K}_p & \mathbf{k}_o^T\mathbf{k}_o \end{bmatrix} = \sigma^2\mathbf{1} \tag{67}$$

where $\sigma > 0$ is a nondimensional scalar and $\mathbf{1}$ is the 3×3 identity matrix. An architecture is considered isotropic as long as its corresponding Jacobian matrix can be rendered isotropic, i.e., with identical singular values, at least at one configuration over the entire workspace [33]. If the isotropy condition does not have a solution, i.e., the manipulator at hand cannot reach a configuration that is isotropic, which is the case at point, then a configuration of minimum condition number is sought.

The condition number of $\mathbf{K}_h$, a dimensionally-homogeneous rectangular matrix, based on the Frobenius norm, is computed as

$$\kappa(\mathbf{K}_h) = \frac{1}{3}\sqrt{\mathrm{tr}(\mathbf{K}_h^T\mathbf{K}_h)\,\mathrm{tr}[(\mathbf{K}_h^T\mathbf{K}_h)^{-1}]} \tag{68}$$

To yield the minimum value of $\kappa(\mathbf{K}_h)$ and the characteristic length of the optimum architecture, we minimize $\kappa^2(\mathbf{K}_h)$ instead, to simplify the ensuing calculating. Thus, the problem is now

$$\min_{\mathbf{x}} \kappa^2(\mathbf{K}_h) \tag{69}$$

subject to three geometric constraints:

$$l > 0,\ l_3 \geq 0,\ \zeta > 0 \tag{70}$$

the design vector $\mathbf{x}$ being given by

$$\mathbf{x} = [x_1, x_2, x_3, x_4]^T \equiv [\alpha, \beta, \zeta, L]^T \tag{71}$$

Let

$$z = \kappa^2(\mathbf{K}_h) \equiv \frac{1}{9}\,\mathrm{tr}(\mathbf{P})\,\mathrm{tr}(\mathbf{P}^{-1}), \quad \mathbf{P} \equiv \mathbf{K}_h^T\mathbf{K}_h \tag{72}$$

when z attains a stationary value, needed for a minimum, its partial derivative with respect to $\mathbf{x}$ vanishes, i.e.,

$$\frac{\partial z}{\partial \mathbf{x}} = \mathbf{0} \tag{73}$$

The foregoing partial derivative is now calculated. To this end, we recall some key relations [55]

$$\frac{\partial[\mathrm{tr}(\mathbf{P})\,\mathrm{tr}(\mathbf{P}^{-1})]}{\partial x_i} \equiv$$
$$\frac{\partial\,\mathrm{tr}(\mathbf{P})}{\partial x_i}\,\mathrm{tr}(\mathbf{P}^{-1}) + \mathrm{tr}(\mathbf{P})\frac{\partial\,\mathrm{tr}(\mathbf{P}^{-1})}{\partial x_i} = \frac{\partial\,\mathrm{tr}(\mathbf{P})}{\partial \mathbf{P}}\frac{\partial \mathbf{P}}{\partial x_i}\,\mathrm{tr}(\mathbf{P}^{-1}) + \mathrm{tr}(\mathbf{P})\frac{\partial\,\mathrm{tr}(\mathbf{P}^{-1})}{\partial \mathbf{P}^{-1}}\frac{\partial \mathbf{P}^{-1}}{\partial x_i} \tag{74}$$

which, after straightforward manipulations, leads to

$$\frac{\partial \mathbf{P}}{\partial x_i}\,\mathrm{tr}(\mathbf{P}^{-1}) - \mathrm{tr}(\mathbf{P})\mathbf{P}^{-1}\frac{\partial \mathbf{P}}{\partial x_i}\mathbf{P}^{-1} = \mathbf{O}, \quad \text{for} \quad i = 1, 2, 3, 4 \tag{75}$$

where $\mathbf{O}$ is the 3×3 zero matrix.

The dimensionally homogeneous matrix $\mathbf{K}_h$ can be expressed in block form as

$$\mathbf{K}_h = \begin{bmatrix} \mathbf{0} & \mathbf{a} & \mathbf{c} \\ \mathbf{b} & \mathbf{0} & \mathbf{d} \end{bmatrix} \tag{76}$$

where

$$\mathbf{a} = \frac{1}{L}\begin{bmatrix} K_{11} \\ K_{21} \end{bmatrix}, \quad \mathbf{b} = \frac{1}{L}\begin{bmatrix} K_{32} \\ K_{42} \end{bmatrix}, \quad \mathbf{c} = \begin{bmatrix} K_{13} \\ K_{23} \end{bmatrix}, \quad \mathbf{d} = \begin{bmatrix} K_{33} \\ K_{43} \end{bmatrix}, \quad \mathbf{0} = \begin{bmatrix} 0 \\ 0 \end{bmatrix} \tag{77}$$

Therefore,

$$\mathbf{P} \equiv \mathbf{K}_h^T \mathbf{K}_h = \begin{bmatrix} \mathbf{0}^T & \mathbf{b}^T \\ \mathbf{a}^T & \mathbf{0}^T \\ \mathbf{c}^T & \mathbf{d}^T \end{bmatrix} \begin{bmatrix} \mathbf{0} & \mathbf{a} & \mathbf{c} \\ \mathbf{b} & \mathbf{0} & \mathbf{d} \end{bmatrix} = \begin{bmatrix} \|\mathbf{b}\|^2 & 0 & \mathbf{b}^T\mathbf{d} \\ 0 & \|\mathbf{a}\|^2 & \mathbf{a}^T\mathbf{c} \\ \mathbf{d}^T\mathbf{b} & \mathbf{c}^T\mathbf{a} & \|\mathbf{c}\|^2 + \|\mathbf{d}\|^2 \end{bmatrix} \equiv \begin{bmatrix} \mathbf{p}_1 & \mathbf{p}_2 & \mathbf{p}_3 \end{bmatrix} \quad (78)$$

whose inverse can be readily derived:

$$\mathbf{P}^{-1} \equiv \frac{1}{\Delta} \begin{bmatrix} (\mathbf{p}_2 \times \mathbf{p}_3)^T \\ (\mathbf{p}_3 \times \mathbf{p}_1)^T \\ (\mathbf{p}_1 \times \mathbf{p}_2)^T \end{bmatrix} = \frac{1}{\Delta} \begin{bmatrix} \|\mathbf{a}\|^2(\|\mathbf{c}\|^2 + \|\mathbf{d}\|^2) - (\mathbf{a}^T\mathbf{c})^2 & (\mathbf{a}^T\mathbf{c})(\mathbf{b}^T\mathbf{d}) & -\|\mathbf{a}\|^2(\mathbf{b}^T\mathbf{d}) \\ (\mathbf{b}^T\mathbf{d})(\mathbf{c}^T\mathbf{a}) & \|\mathbf{b}\|^2(\|\mathbf{c}\|^2 + \|\mathbf{d}\|^2) - (\mathbf{b}^T\mathbf{d})^2 & -\|\mathbf{b}\|^2(\mathbf{a}^T\mathbf{c}) \\ -\|\mathbf{a}\|^2(\mathbf{d}^T\mathbf{b}) & -\|\mathbf{b}\|^2(\mathbf{c}^T\mathbf{a}) & \|\mathbf{a}\|^2\|\mathbf{b}\|^2 \end{bmatrix} \quad (79)$$

where

$$\Delta \equiv \det(\mathbf{P}) = \mathbf{p}_1 \times \mathbf{p}_2 \cdot \mathbf{p}_3 \equiv \|\mathbf{b}\|^2[\|\mathbf{a}\|^2\|\mathbf{c}\|^2 - (\mathbf{c}^T\mathbf{a})^2] + \|\mathbf{a}\|^2[\|\mathbf{b}\|^2\|\mathbf{d}\|^2 - (\mathbf{b}^T\mathbf{d})^2] \quad (80)$$

Thus,

$$\mathrm{tr}(\mathbf{P}) \equiv \|\mathbf{a}\|^2 + \|\mathbf{b}\|^2 + \|\mathbf{c}\|^2 + \|\mathbf{d}\|^2 \quad (81)$$

$$\mathrm{tr}(\mathbf{P}^{-1}) \equiv \frac{1}{\Delta}[\|\mathbf{a}\|^2(\|\mathbf{b}\|^2 + \|\mathbf{c}\|^2 + \|\mathbf{d}\|^2) + \|\mathbf{b}\|^2(\|\mathbf{c}\|^2 + \|\mathbf{d}\|^2) - (\mathbf{a}^T\mathbf{c})^2 - (\mathbf{b}^T\mathbf{d})^2] \quad (82)$$

Substituting Eqs. (78), (79), (81) and (82) into Eq. (75), a system of four equations is obtained. To find the optimum solution, the architecture of the robot is given as $l = 0.6$ m, $l_3 = 0.4$ m, $f_1 = 0.3$ m, $d = 0.1$ m, $e = 0$ m and the initial guess of $\mathbf{x}$, including both the configuration variables α, β, ζ and the characteristic length L, were assigned as

$$\mathbf{x}_{\text{init}} = [0, 0, 0.2, 0.2]^T \quad (83)$$

The Newton-Raphson method was implemented to obtain the optimum. It should be noted that a direct-search method, Nelder-Mead simplex, not relying on gradients, can also be used to solve the foregoing optimization problem with similar results, although it takes a greater number of iterations to converge.

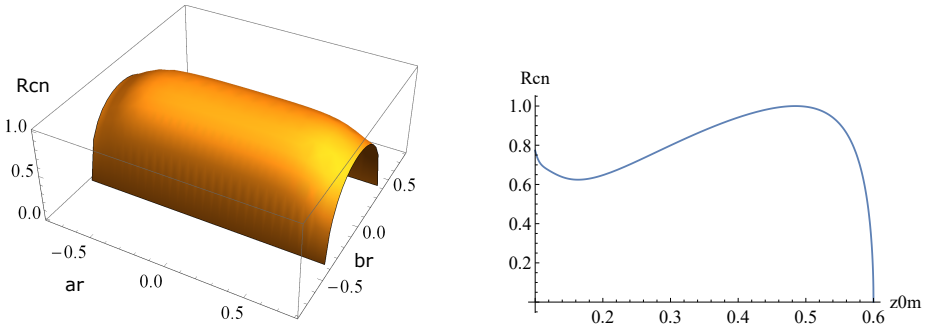

(a) in case of $\zeta = 0.4845$ m (b) in case of $\alpha = 0, \beta = 0$

Figure 7: Reciprocal of condition number of Jacobian matrix

In this case, Mathematica reports a time of 0.2031 s and 1.2969 s for Newton-Raphson method and Nelder-Mead simplex method, respectively. The results thus obtained are displayed below:

$$\mathbf{x}_{\text{opt}} = [0, 0, 0.3, 0.2496]^T \tag{84}$$

whose last component, the characteristic length, is

$$L = 0.2496 \text{ m} \tag{85}$$

Using this number to homogenize the Jacobian of the robot, with the optimum architectural parameters and postural variables, the minimum condition number of interest is obtained as

$$\kappa_{\text{min}} = 1.00013 \approx 1.0 \tag{86}$$

It is noteworthy that the value of ζ obtained via the minimization of the condition number of $\mathbf{K}$ is different from its counterpart when minimizing the condition number of $\mathbf{J}_h$, as given in Eq. (64). Thus, the position $\zeta = 0.3$ m here, should not be taken for granted as the value at the optimum posture.

Moreover, if a tool, with a length h, is added at the said point P, the condition number of the resulting Jacobian, mapped from joint-rates to the new tool-head velocity, will change accordingly. Thus the aforementioned method is used to obtain the optimum length of the tool; the result obtained numerically is

$$h = 0.2874 \text{ m} \tag{87}$$

which yields a minimum condition number

$$\kappa_{\text{min}} = 1.0270 \approx 1.0 \tag{88}$$

which is quite close to isotropy. Now, as tools are usually obtained off-the-shelf, the user is not in a position to fix their length. The logical approach here is to modify the MP so as to accommodate the tool in such a way that its protrusion below the bottom of the MP be as close as possible to the optimum found above.

7.3. Kinetostatic Conditioning Index: KCI

Hence, with the results of optimum posture based on the minimum condition number, the KCI of the PKM is

$$\mathrm{KCI} = 99.9869\% \tag{89}$$

One can readily conclude that the manipulator is closest to isotropy at a configuration given by $\zeta = 0.4845$ m, $\alpha = 0, \beta = 0$. Notice that the value of ζ is different from that of Eq. (84).

7.4. Global Conditioning Index: GCI

In order to evaluate the GCI, we resort to a numerical method because of the complexity of the expression of the condition number [49]. Moreover, since $1/\kappa$ approaches zero at points near singularities, sample points near singularities have a reduced impact on the result of the numerical computation of the GCI. Therefore, a simplified numerical approach was introduced to approximately calculate the GCI by a discrete sum [16]:

$$\mathrm{GCI} \approx \frac{1}{N} \sum_{i}^{N} \frac{1}{\kappa_i} \tag{90}$$

where the workspace has been discretized into a set of N points, κ_i being the value of κ evaluated at the ith point. Thus the result obtained numerically is

$$\mathrm{GCI} = 0.7447 \tag{91}$$

8. Conclusions

A systematic kinematics-cum-dexterity analysis of a novel three-dof redundantly-actuated PKM was reported. Firstly, the mobility of the mechanism is analyzed by means of Lie-group algebra. Then, closed-form solutions for the inverse-displacement problem are obtained, whereas more complex direct-displacement relations are derived in the form of a sixth-degree polynomial whose roots at a given set of actuated joint variables call for a numerical method. Moreover, the velocity analysis is conducted before analyzing the four types of singularities. In terms of characteristics of the Jacobian matrix, the condition number as well as the KCI and the GCI, are used to characterize the robot dexterity. We cope with the dimensionally inhomogeneity of the Jacobian matrices by means of the characteristic length using the Newton-Raphson method. It was shown that the KCI of the mechanism is close to its lower bound of unity, while its GCI is close to 75%, or quite acceptable.

Acknowledgements

The first author would like, first, to acknowledge the China Scholarship Council (CSC) (No. 201708330573) and the Department of Education of Zhejiang Province (Y201430657) for their financial support. Then, the same author acknowledges the use of the research facilities at the Centre for Intelligent Machines at McGill University. The work was supported by: the National Science Foundation of China (NSFC) under Grant Nos. 51525504 and U1713202; and Natural Science Foundation of Zhejiang Province under Grant LZ14E050005. The second author acknowledges the support of Natural Sciences and Engineering Research Council of Canada (NSERC) through its Postdoctoral Fellowship Program. The third author acknowledges NSERC's support through Grant No. 4532-2010.

References

References

[1] F. Pierrot, V. Nabat, O. Company, S. Krut, P. Poignet, Optimal design of a 4-dof parallel manipulator: From academia to industry, IEEE Transactions on Robotics 25 (2) (2009) 213–224.

[2] J.-P. Merlet, Parallel Robots, Vol. 128, Springer Science & Business Media, 2006.

[3] J.-P. Merlet, C. Gosselin, T. Huang, Parallel mechanisms, in: B. Siciliano, O. Khatib (Eds.), Springer Handbook of Robotics, Springer, 2016, Ch. 18.

[4] B. Siciliano, The Tricept robot: Inverse kinematics, manipulability analysis and closed-loop direct kinematics algorithm, Robotica 17 (4) (1999) 437–445.

[5] J. Wahl, Articulated tool head, US Patent 6431802 (2002).

[6] M. Zoppi, D. Zlatanov, R. Molfino, Kinematics analysis of the Exechon tripod, in: ASME 2010 international design engineering technical conferences and computers and information in engineering conference, American Society of Mechanical Engineers, 2010, pp. 1381–1388.

[7] Z. M. Bi, Y. Jin, Kinematic modeling of Exechon parallel kinematic machine, Robotics and Computer-Integrated Manufacturing 27 (1) (2011) 186–193.

[8] Y. Ni, B. Zhang, Y. Sun, Y. Zhang, Accuracy analysis and design of A3 parallel spindle head, Chinese Journal of Mechanical Engineering 29 (2) (2016) 239–249.

[9] A. Yaşır, G. Kiper, Structural synthesis of 2R1T type mechanisms for minimally invasive surgery applications, in: International Workshop on Computational Kinematics, Springer, 2017, pp. 31–38.

[10] H. Wang, W. Li, H. Liu, J. Zhang, S. Liu, Conceptual design and dimensional synthesis of a novel parallel mechanism for lower-limb rehabilitation, Robotica (2018) 1–12.

[11] L. Huang, C. Guang, Y. Yang, P. Su, Type synthesis of parallel 2R1T remote center of motion mechanisms based on screw theory, in: MATEC Web of Conferences, Vol. 95, EDP Sciences, 2017, p. 08009.

[12] Y. Xu, D. Zhang, J. Yao, Y. Zhao, Type synthesis of the 2R1T parallel mechanism with two continuous rotational axes and study on the principle of its motion decoupling, Mechanism and Machine Theory 108 (2017) 27–40.

[13] Q. Li, J. M. Hervé, Type synthesis of 3-dof rpr-equivalent parallel mechanisms, IEEE Transactions on Robotics 30 (6) (2014) 1333–1343.

[14] T. Fu, X. Han, Y. Zhu, H. Ding, Type synthesis of 2R1T parallel mechanism based on Lie group theory, Transactions of Beijing Institute of Technology 11 (2014) 002.

[15] Y. Song, P. Han, P. Wang, Type synthesis of 1T2R and 2R1T parallel mechanisms employing conformal geometric algebra, Mechanism and Machine Theory 121 (2018) 475–486.

[16] Y. Li, Q. Xu, Kinematic analysis of a 3-prs parallel manipulator, Robotics and Computer-Integrated Manufacturing 23 (4) (2007) 395–408.

[17] E. Cuan-Urquizo, E. Rodriguez-Leal, Kinematic analysis of the 3-cup parallel mechanism, Robotics and Computer-Integrated Manufacturing 29 (5) (2013) 382–395.

[18] M. A. Hosseini, Kinematic synthesis of a novel rapid spherical crs/pu parallel manipulator, Mechanism and Machine Theory 93 (2015) 26–38.

[19] L. Wang, H. Xu, L. Guan, Optimal design of a 3-puu parallel mechanism with 2R1T dofs, Mechanism and Machine Theory 114 (2017) 190–203.

[20] L. Xu, Q. Li, J. Tong, Q. Chen, Tex3: An 2R1T parallel manipulator with minimum dof of joints and fixed linear actuators, International Journal of Precision Engineering and Manufacturing 19 (2) (2018) 227–238.

[21] L. Xu, X. Zhu, W. Ye, Q. Li, Q. Chen, Kinematic analysis and dimensional synthesis of a new 2R1T parallel kinematic machine, in: ASME 2018 International Design Engineering Technical Conferences and Computers and Information in Engineering Conference, American Society of Mechanical Engineers, 2018, pp. V05AT07A030–V05AT07A030.

[22] H. de la Torre, E. Rodriguez-Leal, Instantaneous kinematics analysis via screw-theory of a novel 3-crc parallel mechanism, International Journal of Advanced Robotic Systems 13 (3) (2016) 128.

[23] C. Gosselin, L.-T. Schreiber, Redundancy in parallel mechanisms: A review, Applied Mechanics Reviews 70 (1) (2018) 010802.

[24] A. Müller, On the terminology and geometric aspects of redundant parallel manipulators, Robotica 31 (1) (2013) 137–147.

[25] J.-P. Merlet, Redundant parallel manipulators, Laboratory Robotics and Automation 8 (1) (1996) 17–24.

[26] S. Kock, W. Schumacher, A parallel xy manipulator with actuation redundancy for high-speed and active-stiffness applications, in: Proceedings. 1998 IEEE International Conference on Robotics and Automation, Vol. 3, IEEE, 1998, pp. 2295–2300.

[27] M. Gouttefarde, C. Gosselin, Wrench-closure workspace of six-dof parallel mechanisms driven by 7 cables, Transactions of the Canadian Society for Mechanical Engineering 29 (4) (2005) 541–552.

[28] L. Wang, J. Wu, J. Wang, Z. You, An experimental study of a redundantly actuated parallel manipulator for a 5-dof hybrid machine tool, IEEE/ASME Transactions on Mechatronics 14 (1) (2009) 72–81.

[29] J. Wang, J. Wu, T. Li, X. Liu, Workspace and singularity analysis of a 3-dof planar parallel manipulator with actuation redundancy, Robotica 27 (1) (2009) 51–57.

[30] L. Xu, Q. Li, N. Zhang, Q. Chen, Mobility, kinematic analysis, and dimensional optimization of new three-degrees-of-freedom parallel manipulator with actuation redundancy, Journal of Mechanisms and Robotics 9 (4) (2017) 041008.

[31] D. Chakarov, Study of the antagonistic stiffness of parallel manipulators with actuation redundancy, Mechanism and Machine Theory 39 (6) (2004) 583–601.

[32] M. Luces, J. K. Mills, B. Benhabib, A review of redundant parallel kinematic mechanisms, Journal of Intelligent & Robotic Systems 86 (2) (2017) 175–198.

[33] J. Angeles, Fundamentals of Robotic Mechanical Systems Theory, Methods, and Algorithms, Springer, 2014.

[34] J. J. Craig, Introduction to Robotics: Mechanics and Control, Vol. 3, Pearson/Prentice Hall Upper Saddle River, NJ, USA:, 2005.

[35] J. M. Hervé, Analyse structurelle des mécanismes par groupe des déplacements, Mechanism and Machine Theory 13 (4) (1978) 437–450.

[36] J. Angeles, The qualitative synthesis of parallel manipulators, ASME Journal of Mechanical Design 126 (4) (2004) 617–624.

[37] S. Caro, W. A. Khan, D. Pasini, J. Angeles, The rule-based conceptual design of the architecture of serial schönflies-motion generators, Mechanism and Machine Theory 45 (2) (2010) 251–260.

[38] Q. Li, Z. Huang, J. M. Hervé, Type synthesis of 3R2T 5-dof parallel mechanisms using the Lie group of displacements, IEEE Transactions on Robotics and Automation 20 (2) (2004) 173–180.

[39] J. M. Hervé, The Lie group of rigid body displacements, a fundamental tool for mechanism design, Mechanism and Machine theory 34 (5) (1999) 719–730.

[40] L.-W. Tsai, Robot Analysis: the Mechanics of Serial and Parallel Manipulators, John Wiley & Sons, 1999.

[41] C. Gosselin, J. Angeles, Singularity analysis of closed-loop kinematic chains, IEEE Transactions on Robotics and Automation 6 (3) (1990) 281–290.

[42] D. Zlatanov, I. A. Bonev, C. Gosselin, Constraint singularities of parallel mechanisms, in: Robotics and Automation, 2002. Proceedings. ICRA'02. IEEE International Conference on, Vol. 1, IEEE, 2002, pp. 496–502.

[43] C.-H. Choi, H.-S. Park, S.-H. Kim, H.-J. Lee, J.-K. Lee, J.-S. Yoon, B.-S. Park, A manipulator workspace generation algorithm using a singular value decomposition, in: Control, Automation and Systems, 2008. ICCAS 2008. International Conference on, IEEE, 2008, pp. 163–168.

[44] S. Patel, T. Sobh, Manipulator performance measures-a comprehensive literature survey, Journal of Intelligent & Robotic Systems 77 (3-4) (2015) 547–570.

[45] T. Yoshikawa, Manipulability of robotic mechanisms, The International Journal of Robotics Research 4 (2) (1985) 3–9.

[46] J. K. Salisbury, J. J. Craig, Articulated hands: Force control and kinematic issues, The International Journal of Robotics Research 1 (1) (1982) 4–17.

[47] C. Han, J. Kim, J. Kim, F. C. Park, Kinematic sensitivity analysis of the 3-upu parallel mechanism, Mechanism and Machine Theory 37 (8) (2002) 787–798.

[48] J.-P. Merlet, Jacobian, manipulability, condition number, and accuracy of parallel robots, Journal of Mechanical Design 128 (1) (2006) 199–206.

[49] C. Gosselin, J. Angeles, A global performance index for the kinematic optimization of robotic manipulators, Journal of Mechanical Design 113 (3) (1991) 220–226.

[50] C. Gosselin, The optimum design of robotic manipulators using dexterity indices, Robotics and Autonomous systems 9 (4) (1992) 213–226.

[51] P. Cardou, S. Bouchard, C. Gosselin, Kinematic-sensitivity indices for dimensionally nonhomogeneous Jacobian matrices, IEEE Transactions on Robotics 26 (1) (2010) 166–173.

[52] J. Wang, C. Wu, X.-J. Liu, Performance evaluation of parallel manipulators: Motion/force transmissibility and its index, Mechanism and Machine Theory 45 (10) (2010) 1462–1476.

[53] I. Mansouri, M. Ouali, The power manipulability–a new homogeneous performance index of robot manipulators, Robotics and Computer-Integrated Manufacturing 27 (2) (2011) 434–449.

[54] G. H. Golub, C. F. Van Loan, Matrix Computations, Vol. 3, JHU Press, 2012.

[55] W. H. Beyer, S. M. Selby, CRC Standard Mathematical Tables, Vol. 28, CRC Press Boca Raton, FL, 1984.